






Advantages and Limitations of Landau-Zener Surface Hopping Dynamics

 Nina Tokić,¹  Tomislav Piteša,²  Antonio Prlj,²  Marin Sapunar,^{2,*}  Nađa Došlić^{2,*}

¹ Department of Physics, Faculty of Science, University of Zagreb, Croatia

² Department of Physical Chemistry, Ruđer Bošković Institute, Zagreb, Croatia

* Corresponding authors' e-mail addresses: marin.sapunar@irb.hr, nadja.doslic@irb.hr

RECEIVED: October 11, 2024 * REVISED: December 18, 2024 * ACCEPTED: December 23, 2024

THIS PAPER IS DEDICATED TO THE LATE PROFESSOR TOMISLAV CVITAŠ

Abstract: Theoretical investigation of a wide range of photochemical and photophysical phenomena triggered by light absorption requires the use of nonadiabatic molecular dynamics methods. Among these techniques, surface hopping dynamics has emerged as the most widely used approach for modeling photochemical processes in experimentally relevant molecular systems. The Landau-Zener surface hopping method, a simpler alternative to the well-established Tully's fewest switches surface hopping algorithm, presents a compelling option because it does not require the evaluation of nonadiabatic coupling vectors or time derivative couplings. In this study, we present an adaptive time step version of the LZSH algorithm, that enhances its stability while maintaining computational efficiency. We assessed its performance by applying it to several benchmark systems, including the one-dimensional Tully models and the fully-dimensional DMABN molecule.

Keywords: Nonadiabatic dynamics, Tully models, Landau Zener surface hopping, adaptive time step algorithm.

1. INTRODUCTION

NONADIABATIC molecular dynamics (NAMD) methods constitute an essential theoretical tool for studying a broad range of photochemical and photophysical phenomena triggered by light absorption.^[1] Electronically excited molecules typically undergo various internal conversion pathways, some occurring on timescales as short as tens of femtoseconds. Prototypical ultrafast processes, such as photodissociation, photoisomerization, or charge and energy transfer, generally require considering molecular dynamics across multiple electronic states, thus necessitating theoretical frameworks beyond the Born-Oppenheimer approximation (which assumes that dynamics takes place on a single adiabatic potential energy surface — PES).^[2,3] However, as long as nuclear dynamics involves more than one electronic state, treatment of nonadiabatic effects arising from coupled electron-nuclear motion becomes indispensable.

Three main groups of NAMD approaches are typically used,^[4] differing in ways how nuclear dynamics is treated - quantum, semiclassical, and mixed quantum-

classical - though some methods may lie at the intersection of these classifications. Full quantum dynamics involves propagation of nuclear wavepackets on coupled electronic states.^[5] When converged, these methods provide a numerically exact solutions of the time-dependent Schrödinger equation. However, they are typically computationally cumbersome, despite ongoing efforts to beat the exponential scaling with respect to the number of nuclear degrees of freedom. In practice, quantum dynamics is mainly applicable to systems with few degrees of freedom, with the most prominent method being the Multi-Configuration Time-Dependent Hartree (MCTDH).^[6–8] The semiclassical description of nuclear dynamics, while less rigorous, has been a popular research area for decades, employing classical trajectories that incorporate certain quantum effects. Some notable examples include the works of Miller^[9,10] and others.^[11–13] A remarkable approach that draws on ideas from semiclassical dynamics^[11] but remains formally exact is the full multiple spawning.^[14,15] This approach uses classical dynamics to propagate coupled frozen Gaussian functions on multiple electronic states, with the capability to spawn new

functions in regions of nonadiabatic interaction. In practice, however, it is often applied within a more approximate framework of *ab initio* multiple spawning (AIMS),^[16] which allows for an accurate treatment of nonadiabatic dynamics in polyatomic fully-dimensional molecular systems.

At the other end of the approximation spectrum, mixed quantum-classical methods approximate quantum wave packets using swarms of independent classical trajectories, while treating the electronic part quantum mechanically. Apart from neglecting nuclear quantum effects, mixed quantum-classical methods do not account for the quantum mechanical phase of the electronic wave function or quantum interference effects. This makes them unsuitable for describing phenomena like coherence and interference, which depend on the relative phases of wave functions.^[4] Two main mixed quantum-classical approaches, Ehrenfest and surface hopping,^[17] differ primarily in how they address the following dilemma: Newtonian trajectories are propagated along the gradient of PES, but how to calculate a gradient for dynamics on multiple electronic states? The Ehrenfest approach solves this by propagating dynamics on a single “average” (i.e. weighted) PES, while in trajectory surface hopping (TSH) gradients are calculated for an “active” electronic state with a possibility of surface hops. The TSH algorithm acts as a decision-maker, determining when and how to switch between surfaces. By propagating a swarm of classical trajectories, TSH tries to mimic the motion of nuclear quantum wavepacket, distributing population across the manifold of states akin to the wavepacket splitting. Nevertheless, the implementation of TSH opens up numerous pathways for algorithm development, also raising more general questions about whether individual trajectories should be independent or coupled, whether surface hops should be deterministic or stochastic, how total energy should be conserved, among many other considerations.

Although TSH techniques have been around for many decades, they gained significant popularity after the introduction of Tully’s fewest switches surface hopping (FSSH) algorithm in 1990.^[18] It is no exaggeration to say that since its introduction, FSSH has become the primary workhorse for photochemistry simulations in many experimentally relevant molecular systems in atmospheric chemistry, organic and biochemistry.^[19,20] In a conventional FSSH simulation protocol, an ensemble of independent nuclear trajectories is propagated following Newton’s equations of motions, while simultaneously electronic amplitudes are derived from an electronic Schrödinger-like equation solved along the nuclear pathway. Hopping probabilities are determined based on both the electronic state amplitudes and nonadiabatic coupling vectors, incorporating also a stochastic element. One of the

intentions of Tully’s original algorithm was to achieve internal consistency between the quantum and classical subsystems, specifically, to achieve the equivalence of state populations calculated from the fractions of active trajectories with those populations obtained from the squared electronic amplitudes. However, it was later recognized that achieving this consistency is difficult for many systems.^[21] Standard FSSH procedure tends to be overcoherent, with electronic populations typically being broadly spread across the manifold of states as compared to the “classical” populations.^[22] Many decoherence corrections have been proposed to address this issue.^[23–26] In practice, also, nonadiabatic coupling vectors are often difficult to obtain for many electronic structure methods (e.g., most single-reference methods). As a result, FSSH is frequently implemented using overlap-based time-derivative couplings^[27] and local diabaticization to propagate the electronic quantities.^[28] Additionally, other algorithmic details can significantly impact the results — for instance, the handling of frustrated hops^[29] and the ways to rescale momentum after a successful hop have been subjects of ongoing scrutiny.^[26,30–32] The influence of initial conditions on the dynamics has also been a topic of interest.^[33]

A simpler alternative to FSSH is Landau-Zener surface hopping (LZSH), which is based on the core equation for transition probability in a two-state system, dating back to the 1930s.^[34–37] Although the Landau-Zener probability has been used in the context of TSH since decades ago,^[38] interestingly, LZSH has recently re-emerged in the literature,^[39–44] largely due to its appealing properties. In LZSH, the hopping probability is determined solely based on the topography of the PESs near state crossings, eliminating the need to calculate nonadiabatic couplings. This drastically simplifies the interface between nuclear dynamics and electronic structure, as virtually any electronic structure method can be employed as long as it provides energies and gradients. Furthermore, LZSH works for both adiabatic and diabatic representations^[39] of the PES, whereas FSSH is primarily applicable in the adiabatic representation, as argued by Tully.^[18] Consequently, LZSH can routinely handle intersystem crossing via singlet-triplet transitions (usually treated in spin-diabatic representation),^[22,23] a task that is more challenging for FSSH.^[45,46] Another argument in favor of LZSH is a realization that the outcomes of NAMD primarily depend on the accuracy of the underlying electronic structure methods, while nuclear dynamics is typically not a bottleneck for the accuracy of molecular simulations.^[42] In other words, using sophisticated methods for nuclear dynamics does not guarantee the accuracy of simulated observables as long as we use approximate electronic structure methods.^[47] However, it remains crucial to understand the limitations of different

NAMD methods and to recognize situations in which they may not be the optimal methods of choice.

In this work, we assess the performance of LZSH using two one-dimensional Tully models, representing simple (Tully I) and dual avoided crossings (Tully II).^[18] Furthermore, we examine a fully-dimensional molecular benchmark proposed by Ibele and Curchod.^[48] Specifically, we focus on the so called “molecular Tully model II”, represented by the DMABN (4-*N,N'*-dimethylamino-benzonitrile) molecule. This molecule exhibits characteristics similar to the original Tully II model. DMABN molecule undergoes multiple nonadiabatic transitions between the two lowest singlet excitations, which remain energetically close during the excited-state dynamics.^[49–51] Following the initial ultrafast decay from the second excited state, the system experiences population oscillations that correlate with experimentally measured dual fluorescence. The DMABN benchmark system has been studied^[48] using FSSH, both in its pristine form and with decoherence correction, as well as a more rigorous AIMS approach, which provides a valuable point of comparison for the results obtained with LZSH.

2. METHODS

The starting point for any NAMD approach is solving the time-dependent molecular Schrödinger equation (TDSE)

$$i \frac{\partial}{\partial t} \Psi(\mathbf{r}, \mathbf{R}, t) = \hat{H}_M \Psi(\mathbf{r}, \mathbf{R}, t) \quad (1)$$

in the full nuclear configuration space. The symbols \mathbf{r} and \mathbf{R} denote the coordinates of the electrons and nuclei, respectively. Throughout the work atomic units are employed.

The molecular Hamiltonian

$$\hat{H}_M(\mathbf{r}, \mathbf{R}) = \hat{T}_R + \hat{T}_r + V_{en} + V_{ee} + V_{nn} \quad (2)$$

contains the kinetic energy operators of the nuclei \hat{T}_R and of the electrons, \hat{T}_r , and the potential energy operators describing the electron-nuclei, electron-electron, and nuclei-nuclei interactions. It is common to regroup \hat{H}_M as

$$\hat{H}_M(\mathbf{r}, \mathbf{R}) = \hat{T}_R + \hat{H}_{el}(\mathbf{r}, \mathbf{R}) \quad (3)$$

where \hat{H}_{el} is the electronic Hamiltonian. By solving the Schrödinger equation for fixed-nuclei

$$\hat{H}_{el} \Phi_i(\mathbf{r}; \mathbf{R}) = E_i(\mathbf{R}) \Phi_i(\mathbf{r}; \mathbf{R}) \quad (4)$$

one obtains a set of electronic wave functions, $\Phi(\mathbf{r}; \mathbf{R})$, known as the adiabatic electronic states, which are used to expand the molecular wave function:

$$\Psi(\mathbf{r}, \mathbf{R}, t) = \sum_J X_J(\mathbf{R}, t) \Phi_J(\mathbf{r}; \mathbf{R}), \quad (5)$$

where $X_J(\mathbf{R}, t)$ denotes the time-dependent nuclear wave function in the electronic state J . The Born-Huang^[52]

representation of the molecular wave function (Equation (5)) is fundamental to our interpretation of photophysical and photochemical processes, providing the basis for the conventional picture of time-dependent nuclear wave functions evolving on time-independent PESs. Note that alternative representations of the molecular wave function are also possible.^[53]

By following the usual procedure of inserting the expansion (5) into the TDSE (1), multiplying from the left by $\Phi_J^*(\mathbf{r}; \mathbf{R})$ and integrating over the electronic coordinates \mathbf{r} , one obtains a set of coupled differential equations for the nuclear amplitudes, $X_J(\mathbf{R}, t)$. The direct solution of these coupled equations is a challenging task, as it requires expanding the nuclear wave function into a set of time-independent basis functions and solving the resulting equations of motion for the time-dependent expansion coefficients.^[54] As a result, grid-based methods, including the well-known MCTDH approach,^[6–8] scale exponentially with the number of nuclear degrees of freedom (see Ref. [55]). Additionally, grid-based approaches require precomputed global PESs, which further restrict the scope of problems that can be simulated.

As mentioned in the Introduction, the goal of this work is to compare three approaches for approximating the TDSE on-the-fly: the *ab initio* multiple spawning (AIMS), the fewest switches surface hopping (FSSH), and the Landau-Zener surface hopping (LZSH) method. These methods avoid the need for precomputed global potentials and solve the TDSE in real-time, calculating electronic-state energies and gradients along the nuclear dynamics evolution. Since these approaches have been extensively reviewed in the literature, we will provide only a brief overview here.

2.1 Ab Initio Multiple Spawning

To describe the fundamentals of the AIMS approach, we follow Ref. [56] and present the full multiple spawning method from which AIMS is derived. In full multiple spawning, the nuclear wave function $X_J(\mathbf{R}, t)$ is expanded in a linear combination of multidimensional Gaussian basis functions

$$X_J(\mathbf{R}, t) = \sum_j^{N_j(t)} C_j^J(t) \chi_j^J(\mathbf{R}; \bar{\mathbf{R}}_j^J(t), \bar{\mathbf{P}}_j^J(t), \bar{\mathbf{V}}_j^J(t), \alpha_j^J) \quad (6)$$

where J is the label of the Gaussian basis function with time-dependent position $\bar{\mathbf{R}}_j^J(t)$, momentum $\bar{\mathbf{P}}_j^J(t)$ and phase $\bar{\mathbf{V}}_j^J(t)$. The width α_j^J of the traveling basis function (TBF) is frozen. The phase space centers of TBFs follow classical equations of motion. Using the standard procedure, one first inserts Equation (6) into Equation (5) and subsequently into Equation (1). Then, after multiplying the resulting expression from the left with $\Psi^*(\mathbf{r}, \mathbf{R}, t)$ and integrating over both the electronic and nuclear

coordinates, a coupled system of equations is obtained.

$$\frac{d\mathbf{C}'(t)}{dt} = -i(\mathbf{S}_{II}^{-1}) \left(\left(\mathbf{H}_{II} - i\dot{\mathbf{S}}_{II} \right) \mathbf{C}' + \sum_{J \neq I} \mathbf{H}_{IJ} \mathbf{C}^J \right) \quad (7)$$

where $(\mathbf{S}_{II})_{kl} = \langle \chi_k' | \chi_l' \rangle_{\mathbf{R}}$ is the overlap matrices accounting for the nonorthogonality of the TBF, $(\dot{\mathbf{S}}_{II})_{kl} = \langle \chi_k' | \frac{\partial}{\partial t} | \chi_l' \rangle_{\mathbf{R}}$ and

$$(\mathbf{H}_{IJ})_{kl} = \langle \chi_k' \Phi_I | \hat{H}_M | \chi_l' \Phi_J \rangle_{\mathbf{R}, \mathbf{r}} \quad (8)$$

is an element of the molecular (full) Hamiltonian matrix. From the terms above, we can see that TBFs moving on the same electronic state are coupled together by the nuclear kinetic energy operator and the electronic energy term, while TBFs on different electronic states remain coupled by the nonadiabatic coupling vectors and the second order nonadiabatic couplings. While two nonadiabatic terms are generally non-zero in the adiabatic representation, the second order terms are picked in a narrower part of the configuration space than the first order terms and are usually neglected in the simulations. To “contain” the dimensionality of Equation (7) Martínez *et al.*^[57] introduced a spawning algorithm that optimizes the number of TBFs in each electronic state during the simulation based on the strength of the nonadiabatic coupling between the states. The idea is that as the system passes through a region of nonadiabatic coupling, new TBFs are created on the coupled electronic states. This means one can start with a relatively small number of TBFs and allow the basis set to grow during the simulation, accounting for the non-adiabatic transfer of population between electronic states. Details of the spawning algorithm are given in Refs. [56–58]

Apart from the size of the Hamiltonian matrix, the main limitation of the full multiple spawning method is that it requires integration over the whole nuclear configuration space for each pair of TBFs. In other words, the method still requires precomputed PES. To address this issue, the AIMS method was developed.^[58] AIMS is based on two approximations:

(i) The first-order saddle-point approximation is used to evaluate the multidimensional integrals of the Hamiltonian matrix as

$$\langle \chi_k' | H_{IJ} | \chi_l' \rangle = H_{IJ}(\tilde{\mathbf{R}}) \langle \chi_k' | \chi_l' \rangle \quad (9)$$

where $\tilde{\mathbf{R}}$ is the centroid of the product of TBFs χ_k' and χ_l' . This approximation exploits the semi-local nature of the traveling Gaussian functions and applies to both the diagonal and off-diagonal elements of the Hamiltonian matrix.

(ii) The independent-first-generation approximation sets the initial amplitudes in Equation (6) to one ($C_j'(t_0) = 1$) and instead of propagating a coupled set of equations from

the outset, the TBFs are initially propagated independently. These “parent” TBFs subsequently spawn new TBFs and the coupled set of Equations (7) is propagated. By starting from independent “parent” TBFs and using the saddle-point approximation to evaluate Hamiltonian elements, the method becomes suitable for on-the-fly simulations. However, the propagation of Equation (7) remains numerically demanding, requiring the interface between AIMS and electronic structure methods to strike a balance between accuracy and efficiency.

2.2 Trajectory Surface Hopping Methods

TSH methods rely on the propagation of (independent) classical trajectories initiated in a specified electronic state called the active state. The total wave function is expanded as:

$$\Psi(\mathbf{r}, t; \mathbf{R}) = \sum_J C_J(t) \Phi_J(\mathbf{r}; \mathbf{R}), \quad (10)$$

where $\Phi_J(\mathbf{r}; \mathbf{R})$ is the J -th adiabatic (Born-Oppenheimer) electronic state with associated coefficient $C_J(t)$. Inserting Equation (10) into Equation (1) one obtains a set of coupled differential equations for the coefficients (i.e., amplitudes):

$$\frac{dC_J(t)}{dt} = -C_J(t)E_J + \sum_I C_I \langle \Phi_J(\mathbf{r}; \mathbf{R}) | \frac{d}{dt} | \Phi_I(\mathbf{r}; \mathbf{R}) \rangle. \quad (11)$$

The time-derivative couplings \mathcal{D}_{IJ} can be expressed in terms of the nuclear velocities as:

$$\begin{aligned} \mathcal{D}_{IJ} &= \langle \Phi_J(\mathbf{r}; \mathbf{R}) | \frac{d}{dt} | \Phi_I(\mathbf{r}; \mathbf{R}) \rangle \\ &= \langle \Phi_J(\mathbf{r}; \mathbf{R}) | \nabla_{\mathbf{R}} | \Phi_I(\mathbf{r}; \mathbf{R}) \rangle \frac{d\mathbf{R}}{dt} \end{aligned} \quad (12)$$

where $\nabla_{\mathbf{R}}$ denotes the gradient with respect to the nuclear coordinates. From Equations (11) and (12), it is evident how the nuclear dynamics influence electronic motion. When trajectory passes through a region of strong nonadiabatic coupling, the population of the coupled but unoccupied electronic state rises. However, the nuclear motion is still not affected by the electronic motion, as it proceeds only on one active state. In other words, the increase in electronic population of an unoccupied electronic state does not reflect in the nuclear dynamics. The goal of TSH algorithms is to (re)introduce the feedback between electronic and nuclear motion.

In this work we consider two variants of TSH.

(i) FSSH algorithm is by far the most widely used TSH algorithm, despite the fact that it cannot be rigorously derived.^[17,18]

In FSSH, variations in the electronic state populations along a nuclear trajectory are used to determine when a nuclear trajectory switches from one active state to

another. The hopping probability from a state I to a state J reads:

$$P_{FSSH}^{I \rightarrow J} = \max \left\{ 0, -\frac{d |C_{I \rightarrow J}(t)|^2}{dt} \right\} \\ = \max \left\{ 0, \frac{2\mathcal{D}_{IJ}(t)\text{Re}[C_J^*(t)C_I(t)]}{|C_I(t)|^2} dt \right\}. \quad (13)$$

Therefore, hops between electronic states take place when the population of the currently active state decreases and the maximum value criterion ensures that the probability remains positive at all times. After a successful hop, the momenta are scaled to ensure the conservation of total energy.

(ii) LZSH algorithm is a simpler alternative to FSSH. Several derivations of the Landau-Zener (LZ) formula are available in the literature [34,35,59–61] (for more recent derivations, see Refs. [62] and [63]). In contrast to FSSH, which provides the hopping probability between two adiabatic electronic states, the conventional LZ formula gives the transition probability between two diabatic electronic states

$$P_{IJ}^{LZ} = \exp \left(-\frac{2\pi H_{IJ}^2}{\hbar v |H'_{II} - H'_{JJ}|} \right), \quad (14)$$

where H_{II} and H_{JJ} are diagonal matrix elements of the Hamiltonian, and H'_{II} and H'_{JJ} their derivatives with respect to nuclear coordinates. Importantly, the LZ expression was derived under the assumption of linear dependence of the two crossing potentials on nuclear coordinates. The off-diagonal element H_{IJ} is considered constant and v is the atomic velocity vector. The transition probability is calculated at the crossing point of the two potentials in the nonadiabatic region \mathbf{R}_c . The interpretation of the LZ formula is straightforward - the nonadiabatic transition probability, i.e., the probability to remain in the initial diabatic state is low when the diabatic potentials have similar slopes and the relative velocity of the atoms is small.

It goes without saying that Equation (14) is not suitable for on-the-fly simulations as diabatic PESs are not readily available from standard electronic structure codes. However, following Belyaev and Lebedev^[64] Equation (14) can be recast in the adiabatic form as following:

$$P_{IJ}^{LZ} = \exp \left(-\frac{\pi}{2\hbar} \sqrt{\frac{Z_{IJ}^3}{\ddot{Z}_{IJ}}} \right), \quad (15)$$

where Z_{IJ} is the splitting between the adiabatic potentials U_I and U_J and \ddot{Z}_{IJ} is the second time derivative of the energy gap. The hopping probability is computed when the gap Z_{IJ} between the two adiabatic potentials reaches a minimal value.

While the LZ formula (15) can now be employed in on-the-fly TSH simulations, it is useful to express it in terms that are actually evaluated along a trajectory, namely, the adiabatic energies at discrete time steps.^[65] The second derivative of the energy gap is calculated when the gap minimum is reached ($t = t_c$) using a three-point finite difference

$$\ddot{Z}_{IJ}(t_c) = \frac{Z_{IJ}(t - \Delta t) + Z_{IJ}(t + \Delta t) - 2Z_{IJ}(t)}{\Delta t^2} = \frac{2d(t)}{\Delta t^2}, \quad (16)$$

where we have defined $d(t) = (Z_{IJ}(t - \Delta t) + Z_{IJ}(t + \Delta t) - 2Z_{IJ}(t)) / 2$ as the average change in the gap between the time steps around the minimum. We can insert this form back into Equation (15) to obtain the LZ formula for finite time steps

$$P_{IJ}^{LZ} = \exp \left(-\frac{\pi}{2\hbar} \sqrt{\frac{Z_{IJ}^3(t)\Delta t^2}{2d(t)}} \right) \quad (17)$$

An obvious source of error in the expression (17) is that the time at which the probability should be evaluated (t_c) has been replaced by the time t at the nearest discrete time step. Since the probability is an exponential function of the values evaluated at this time, it is expected to be highly sensitive to these values. Luckily, since the probability has to be evaluated only at points where a minimum of the energy gap between two surfaces is encountered, an adaptive time step procedure can be employed to enhance the numerical stability of the method without significantly increasing the computational cost.

The adaptive time step procedure implemented for LZSH^[65] involves an optimization of the gap $Z_{IJ}(t)$ between potential energy curves using a bisection method. To avoid unnecessary evaluations of the PES, we assume that the gap minimum $Z_{IJ}(t_c)$ lies in the range $Z_{IJ}(t) - d \leq Z_{IJ}(t_c) \leq Z_{IJ}(t)$. Inserting these limits into Equation (17), we obtain an estimate of the upper and lower bound of the LZ hopping probability. When this error estimate is larger than certain threshold value (typically 1%), we bisect the time step and evaluate the probability again. However, when reducing the time step for the calculation, one needs to be mindful of the fact that the energies of the states are usually only calculated up to a certain precision σ , which complicates the considerations. The “noise” in the results due to the finite precision of the calculated values can lead to numerical issues if a time step that is too small is chosen, especially in the evaluation of the second derivative. To avoid numerical issues due to the precision of the calculated energies, the second derivative is only recalculated if $d \geq 20\sigma$, while the bisection procedure is not performed at all if $d \leq 2\sigma$. Pseudocode for the decision on when to change the time step is given in Figure 1.

2.3 Computational details

The LZSH algorithm was tested on Tully models I and II.^[18] For these one-dimensional two-surface models, sets of 2000 trajectories for each velocity and/or time step were initiated with the position x chosen randomly in the $[-6, -5]$ range. The trajectories were terminated when the particle left the interaction region ($|x| > 6.1$). The trajectories were then sorted based on their final position (transmission for $x > 6$ and reflection for $x < -6$) and final state. To test the robustness of the adaptive time step algorithm, for some calculations using model I, random noise (a uniform random number $-0.5\sigma \leq r \leq 0.5\sigma$) was added to each of the evaluated energies and gradients to simulate the effect of the electronic structure calculations precision on the performance of the algorithm. The exact parameters used for both models were taken from Ref. [18]. Unless otherwise noted, a time step of 0.5 fs was used for model I, respectively. A time step of 0.1 fs was used for model II, which was determined to be stable for the chosen set of parameters without employing the adaptive time step algorithm.

To assess the accuracy of LZSH for molecular systems, we investigate the photodynamics of DMABN, an example of the molecular Tully model II.^[48] The AIMS and FSSH results for DMABN were taken from Ref. [48]. The simulations were performed in the manifold of the four lowest singlet states ($S_0 - S_3$), starting from the S_2 state over a 200 fs time window. Energy and gradient calculations were carried out using the Gaussian09 program,^[66] employing the linear-response TDDFT method^[67-69] within the Tamm-Dancoff approximation. The long-range corrected LC-PBE functional,^[70,71] with a range-separation parameter of 0.3 a.u.⁻¹, was used in combination with the 6-31G basis set. A time step of 0.5 fs was employed with a probability threshold for the adaptive time step procedure set at 5 %. With this setting, an average of only 1.2 extra time steps were added per trajectory.

In AIMS simulations, a total of 21 initial coordinates and momenta were sampled from a ground-state Wigner distribution. In FSSH simulations, the same initial conditions as in the AIMS dynamics were employed, but each trajectory was repeated 10 times with different random seeds to allow exploration of a larger section of the configuration space. Corresponding set of initial conditions is referred to as set A. FSSH simulations were performed with and without an energy-based decoherence correction,^[24] but we only use the former one for comparison with LZSH.

In our LZSH simulations, we employed the same electronic structure method and initial conditions outlined above. However, another set of initial conditions was also

used — in addition to set A, we conducted simulations using set B, which consisted of 210 distinct initial conditions sampled from the ground-state Wigner distribution.

```
def check_bisect(s0, s1, s2):
    # The input variables contain data from the three
    # steps between which a gap minimum was detected.
    d = (s0.gap + s2.gap - 2*s1.gap)/2
    if sd_not_evaluated or d > 20 * sigma:
        s1.second_deriv = eval_sec_deriv(s0, s1, s2)
        sd_not_evaluated = False
    prob_min = eval_lz_prob(s1.gap, s1.second_deriv)
    prob_max = eval_lz_prob(s1.gap - d, s1.second_deriv)
    # Check for situations where bisection is not needed:
    if prob_max - prob_min < prob_threshold:
        return prob_min
    if s2.time - s1.time <= min_dt:
        return prob_min
    if d <= 2*sigma:
        return prob_min
    # Bisection is needed, check where to add the time step:
    if s1.time - s0.time >= s2.time - s1.time:
        new_time = (s1.time - s0.time) / 2
    else:
        new_time = (s2.time - s1.time) / 2
    return new_time
```

Figure 1. Pseudocode to check whether a new time step should be added in the adaptive time step algorithm. If a bisection is needed, a new substep calculation is performed at the requested time, and this function will be called again when the gap is found between the new substep and the previous calculations. Otherwise, the hopping probability is evaluated without performing extra calculations.

3. RESULTS AND DISCUSSION

3.1 1D Tully models I and II

In Figure 2 we evaluate the performance of the LZSH algorithm for Tully's model I, representing a simple avoided crossing. Despite its simplicity, model I is already useful to illustrate the strengths and weaknesses of the LZSH approach. A comparison between the FSSH and LZSH algorithms is shown in panel (b).

We see that the LZSH algorithm (with the adaptive time step procedure) correctly describes the behavior for large initial momenta k , but significantly overestimates the hopping probability for low initial momenta. For $k < 8.9$ the particle does not have enough energy to leave the well on the upper surface so in case of jumps to the upper surface it remains temporarily trapped before hopping back down to the lower surface. At first glance this behavior is correctly captured by the LZSH algorithm.

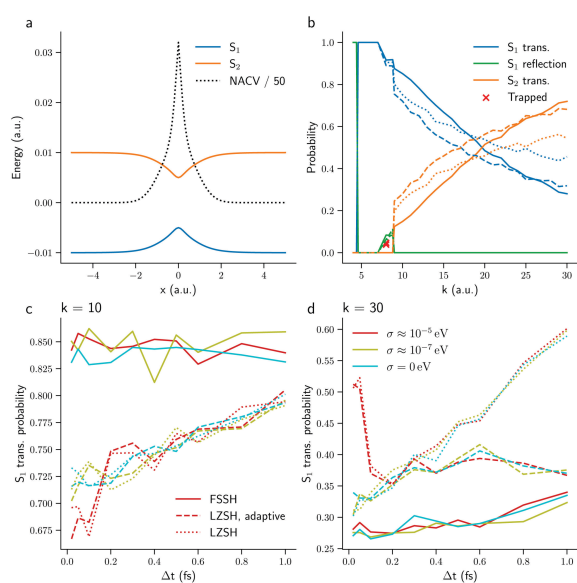


Figure 2. (a) Potential energy curves for Tully model I. (b). Transmission and reflection probabilities calculated using the FSSH (full lines) and the LZSH method with (dashed lines) and without (dotted lines) the adaptive time step procedure. (c) and (d) Probability of transmission on the lower surface for initial momenta $k = 10$ and $k = 30$ a.u. calculated for different noise levels (colors) and with different time steps using the FSSH and LZSH methods.

However, trajectories that reach this well at the LZSH level remain trapped for significantly longer time than equivalent FSSH trajectories, with some trajectories remaining in the well even after the 10000 fs simulation time. These trajectories are denoted with crosses in Figure 2. This unphysical trapping is a limitation of the method itself and not caused by numerical issues, however, it is expected to be less relevant for molecules with many degrees of freedom.

Figures 2(c) and 2(d) explore the stability issue of the adiabatic LZ formula evaluated at discrete time steps. The probability of transmission on the lower surface is calculated using trajectories with time steps between $\Delta t = 0.02$ and $\Delta t = 1.0$ fs. For both high and low initial momenta, we see that the probability at the LZSH level changes with the time step used in the calculation. This indicates that the method is less stable than FSSH with respect to the time step used, which was anticipated for the reasons explained above. For high initial momenta, where the problem is most significant, the adaptive time step procedure enhances the method's stability to match that of FSSH. When random noise is introduced into the calculation, we observe that the LZSH procedure generates substantial errors abruptly when the time step is reduced below a certain threshold. The adaptive time step

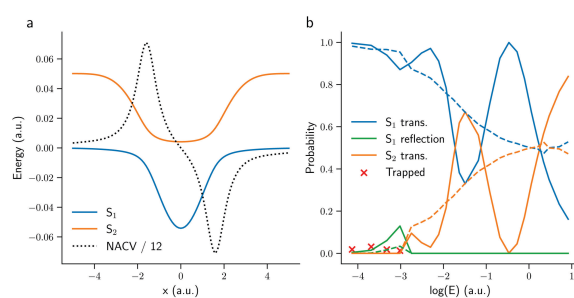


Figure 3. (a) Potential energy curves for Tully model II. (b) Transmission and reflection probabilities calculated using the FSSH (full lines) and the LZSH method (dashed lines).

procedure detailed above successfully avoids reducing the time step to the point where such problems can occur. We also see that when the adaptive time step procedure is employed, errors due to the time step are similar to those in FSSH for large kinetic energies where the LZSH algorithm would otherwise be completely unstable for large time steps. This allows us to choose the same time step for LZSH as we would for FSSH while assuming that the main source of the error is from the LZ probability itself and not due to numerical issues.

Next, we examine the performance of the LZSH algorithm for Tully's dual avoided crossing model (model II) shown in Figure 3(a). This model is significantly more challenging because it exhibits quantum interference effects. These effects are completely neglected in LZSH and, consequently, the oscillations present in FSSH results are not seen at all with LZSH (for a recent study see Ma *et al.*^[72])

In the low kinetic energy (E) region, we encounter a problem with population trapping similar to the one observed with model I and, overall, the reflection probability is greatly underestimated for LZSH. On the other hand, the LZSH results do correctly follow the general trend of the populations after transmission. Nevertheless, the interference effects will not be relevant for the molecular version of this model (see below) due to the increased number of degrees of freedom.

3.2 Molecular Tully model II

To move beyond the one-dimensional models and assess the performance of LZSH for a molecule in its full dimensionality, we shift our focus to the DMABN molecule, which serves as an example of the molecular Tully model II.^[48]

The upper panel of Figure 4 shows the time-dependent potential energies of the ground and three lowest singlet states of DMABN along a representative nonadiabatic trajectory initiated in bright S_2 state. The trajectory is computed using the LZSH method.

The changes in the currently populated state (dots) stem from multiple nonadiabatic transitions. The dominant

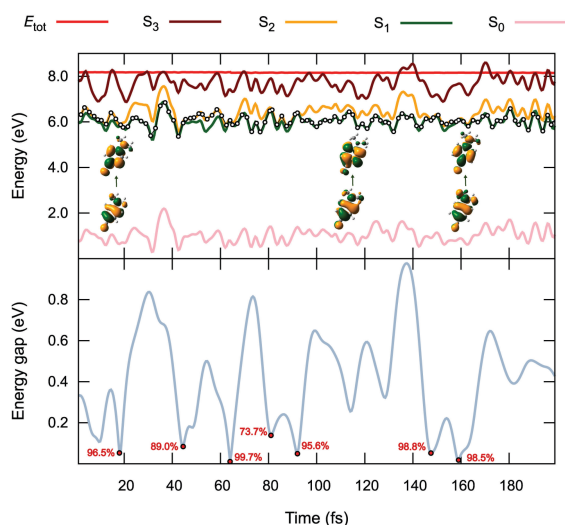


Figure 4. Top: Time evolution of the potential energy for the ground state (S_0 , pink), S_1 (green), S_2 (yellow), and S_3 (maroon) states along a representative nonadiabatic trajectory of DMABN, computed using the LZSH method. The active state is marked with dots. Insets display the dominant NTO pairs at selected time points. Bottom: Time evolution of the $S_2 - S_1$ potential energy gap along the trajectory, with the corresponding LZ transition probabilities.

natural transition orbital (NTO) pairs shown in the insets clearly indicate that hops between adiabatic states (may) also result in a change of the diabatic state. Hops between the two states occur at 18.00 fs, 44.50 fs, 64.00 fs, 81.00 fs, 92.00 fs, 147.50 fs, and 159.00 fs.

The lower panel shows that the hopping points correspond to the local minima of the energy gap between the S_2 and S_1 . Comparison of energy gaps at the hopping points (0.0527 eV, 0.0838 eV, 0.0105 eV, 0.1383 eV, 0.0491 eV, 0.052 eV, and 0.0179 eV) and the corresponding Landau-Zener probabilities (96.5 %, 89.0 %, 99.7 %, 72.7 %, 95.6 %, 98.8 %, and 98.5 %) illustrates that gaps have a decisive influence on hopping probabilities. Therefore, the performance of LZ algorithm will also depend on the ability of the electronic structure method to accurately describe avoided crossings between adiabatic surfaces.

We now focus on the ensemble of trajectories initiated in the bright S_2 state. Figure 5 compares the time-dependent populations of the four lowest electronic states, calculated using initial conditions from set A ($N_{traj} = 21$ trajectories, each initiated with 10 different random seeds) and set B ($N_{traj} = 210$ trajectories).

The rapid depopulation of the initially-excited S_2 state is evident in both cases, although relaxation appears to occur slightly faster for set B. Notably, set A exhibits a more pronounced repopulation of the S_2 state, with distinct

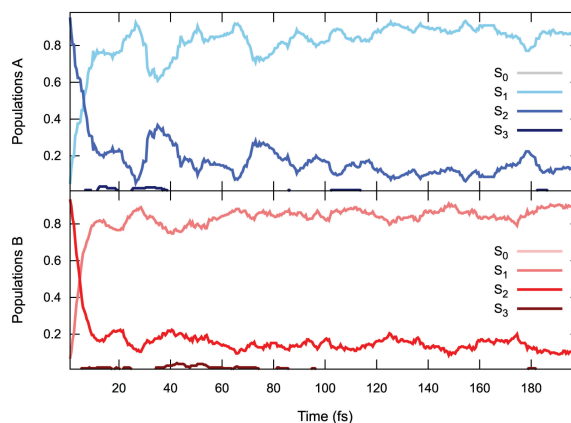


Figure 5. Populations of the four lowest adiabatic states ($S_0 - S_3$) of DMABN computed with LZSH. Top: initial conditions for set A. Bottom: initial conditions for set B. For details on initial condition sets A and B see text.

oscillations between the S_2 and S_1 populations that gradually decay over time.

Furthermore, we can compare LZSH simulations with the results from AIMS method (dark blue), which in this case may be considered as a theoretical best estimate, and the FSSH (light blue). FSSH simulations were conducted using initial conditions from set A, incorporating the decoherence correction, and they are referred to as dTSH following Ref. [48].

According to the AIMS and dTSH results, after the initial excitation to the S_2 state, ultrafast relaxation occurs within the first 50 fs of the simulation.^[48] Subsequently, the S_2 population stabilizes around 15 %.

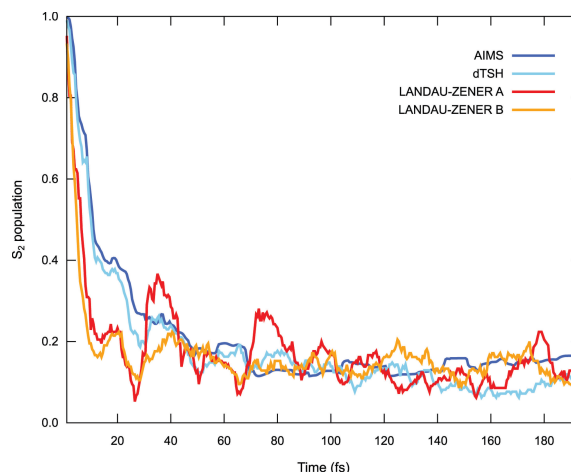


Figure 6. Decay of the population of the S_2 state of DMABN as obtained by different nonadiabatic dynamics methods: AIMS (dark blue), decoherence-corrected FSSH (dTSH, light blue), LZSH with set A initial conditions (Landau-Zener A, red) and with set B initial (Landau-Zener B, orange).

The LZSH method predicts a significantly faster decay of the S_2 state. The population of the S_2 state drops below 20 % within just 10 fs. This is followed by a partial repopulation of the state, and by the end of the simulation time, the LZSH population values fall between those obtained from AIMS and FSSH (dTSH). Considering the choice of initial conditions, it is evident that LZSH yields notably better results using initial conditions from set B. The oscillations observed with set A are likely artifacts resulting from undersampling of the configuration space.

Thus, compared to FSSH, LZSH shows less variation between runs with different random number sequences (i.e. trajectories tend to be more “deterministic”), which should be taken into account when sampling initial conditions.

Overall, we observe that the simple LZSH algorithm, which unlike FSSH does not retain any memory of past transitions (compare Equations (13) and (15)), performs relatively well in the rather challenging case of molecular Tully model II which involves multiple nonadiabatic transitions. However, further investigation is needed to fully understand the rapid depopulation observed at the beginning of the simulation.

4. CONCLUSIONS

In this study, we evaluated the performance of the Landau-Zener surface hopping (LZSH) algorithm for simulating nonadiabatic excited-state dynamics. Since the LZSH algorithm determines hopping probabilities based on the minimum energy gap between electronic states, it is essential to select an appropriate time step for nuclear dynamics. A time step that is too large may overlook the minimum gap, while an excessively small step can result in inefficient calculations. To address this issue, we developed an adaptive time step version of the LZSH algorithm.

We tested the adaptive LZSH algorithm using Tully's one-dimensional models I and II, which include simple and dual crossings between electronic states, as well as the “molecular Tully model II” represented by the DMABN molecule. Our key findings are as follows:

- a) For Tully's model I, the adaptive LZSH algorithm accurately captures the dynamics at high initial momenta but tends to overestimate hopping probabilities at low initial momenta. When random noise was introduced to simulate errors in electronic structure calculations, the algorithm generated incorrect transitions when excessively small time steps were employed. The adaptive time step approach effectively addressed this issue by reducing the time step around the gap minimum by as little as possible to increase the accuracy of the evaluated gap minimum.
- b) For Tully's model II, which is designed to test quantum

interference effects, we observed that while the LZSH algorithm did not replicate the oscillations seen in FSSH, it still accurately followed the overall population trends. However, in certain cases with very low initial momenta, the LZSH method resulted in unphysical trapping of trajectories on the upper surface.

c) For the DMABN molecule, the LZSH algorithm performed well during longer simulation times but deviated from “best estimate” results in the early stage of dynamics. This behavior is reminiscent of LZSH performance for Tully's model I at low kinetic energies, where it also overestimated hopping probabilities.

In summary, the LZSH method is straightforward to integrate with various electronic structure approaches and can be implemented in both adiabatic and diabatic representations, making it a valuable tool for studying photoinduced processes. However, users should be aware of its potential numerical issues. The adaptive time step approach we propose enhances the stability of the LZSH algorithm without significantly increasing the computational cost.

Acknowledgements. The authors acknowledge support from the Croatian Science Foundation (HRZZ) grants HRZZ-IP-2020-02-9932, HRZZ-IP-2022-10-4658 and HRZZ-IP-2020-02-7262.

REFERENCES

- [1] S. Mai, L. González, *Angew. Chem. Int. Ed.* **2020**, *59*, 16832–16846.
<https://doi.org/10.1002/anie.201916381>
- [2] D. J. Tannor, *Introduction to quantum mechanics: a time-dependent perspective*, University Science Books, Sausalito, **2007**.
- [3] J. Michl, V. Bonačić-Koutecký, *Electronic Aspects of Organic Photochemistry*, John Wiley and Sons Ltd, **1990**.
- [4] J. C. Tully, *J. Chem. Phys.* **2012**, *137*, 22A301.
<https://doi.org/10.1063/1.4757762>
- [5] G. A. Worth, L. S. Cederbaum, *Annu. Rev. Phys. Chem.*, **2004**, *55*, 127–158.
<https://doi.org/10.1146/annurev.physchem.55.091602.094335>
- [6] H.-D. Meyer, U. Manthe, L. S. Cederbaum, *Chem. Phys. Lett.* **1990**, *165*, 73–78.
[https://doi.org/10.1016/0009-2614\(90\)87014-I](https://doi.org/10.1016/0009-2614(90)87014-I)
- [7] H.-D. Meyer, *Wiley Interdiscip. Rev. Comput. Mol. Sci.* **2012**, *2*, 351–374.
- [8] G. A. Worth, H.-D. Meyer, H. Köppel, L. Cederbaum, I. Burghardt, *Int. Rev. Phys. Chem.* **2008**, *27*, 569–606.
<https://doi.org/10.1080/01442350802137656>

- [9] W. H. Miller, *J. Phys. Chem. A* **2001**, *105*, 2942–2955. <https://doi.org/10.1021/jp003712k>
- [10] W. H. Miller, *J. Phys. Chem. A* **2009**, *113*, 1405–1415. <https://doi.org/10.1021/jp809907p>
- [11] E. J. Heller, *Acc. Chem. Res.* **1981**, *14*, 368–375. <https://doi.org/10.1021/ar00072a002>
- [12] G. Stock, M. Thoss, *Phys. Rev. Lett.* **1997**, *78*, 578. <https://doi.org/10.1103/PhysRevLett.78.578>
- [13] S. Bonella, D. Coker, *J. Chem. Phys.* **2001**, *114*, 7778–7789. <https://doi.org/10.1063/1.1366331>
- [14] M. Ben-Nun, J. Quenneville, T. J. Martínez, *J. Phys. Chem. A* **2000**, *104*, 5161–5175. <https://doi.org/10.1021/jp994174i>
- [15] B. F. Curchod, T. J. Martínez, *Chem. Rev.* **2018**, *118*, 3305–3336. <https://doi.org/10.1021/acs.chemrev.7b00423>
- [16] B. Mignolet, B. F. Curchod, *J. Chem. Phys.* **2018**, *148*, 134110. <https://doi.org/10.1063/1.5022877>
- [17] J. Tully, in *Modern methods for multidimensional dynamics computations in chemistry*, ed. D. L. Thompson, World Scientific, Singapore, **1998**.
- [18] J. C. Tully, *J. Chem. Phys.* **1990**, *93*, 1061–1071. <https://doi.org/10.1063/1.459170>
- [19] H. Güsten, G. Heinrich, T. Cvitaš, L. Klasinc, B. Ruščić, D. P. Lalas, M. Petrakis, *Atmos. Environ. (1967)*, **1988**, *22*, 1855–1861. [https://doi.org/10.1016/0004-6981\(88\)90074-1](https://doi.org/10.1016/0004-6981(88)90074-1)
- [20] R. Crespo-Otero, M. Barbatti, *Chem. Rev.* **2018**, *118*, 7026–7068. <https://doi.org/10.1021/acs.chemrev.7b00577>
- [21] J.-Y. Fang, S. Hammes-Schiffer, *J. Phys. Chem. A* **1999**, *103*, 9399–9407. <https://doi.org/10.1021/jp991602b>
- [22] T. Nelson, S. Fernandez-Alberti, A. E. Roitberg, S. Tretiak, *J. Chem. Phys.* **2013**, *138*, 224111. <https://doi.org/10.1063/1.4809568>
- [23] C. Zhu, S. Nangia, A. W. Jasper, D. G. Truhlar, *J. Chem. Phys.* **2004**, *121*, 7658–7670. <https://doi.org/10.1063/1.1793991>
- [24] G. Granucci, M. Persico, *J. Chem. Phys.* **2007**, *126*, 134114. <https://doi.org/10.1063/1.2715585>
- [25] G. Granucci, M. Persico, A. Zocante, *J. Chem. Phys.* **2010**, *133*, 134111. <https://doi.org/10.1063/1.3489004>
- [26] J. E. Subotnik, N. Shenoi, *J. Chem. Phys.* **2011**, *134*, 024105. <https://doi.org/10.1063/1.3506779>
- [27] S. Hammes-Schiffer, J. C. Tully, *J. Chem. Phys.* **1994**, *101*, 4657–4667. <https://doi.org/10.1063/1.467455>
- [28] G. Granucci, M. Persico, A. Toniolo, *J. Chem. Phys.* **2001**, *114*, 10608–10615. <https://doi.org/10.1063/1.1376633>
- [29] A. W. Jasper, D. G. Truhlar, *Chem. Phys. Lett.* **2003**, *369*, 60–67. [https://doi.org/10.1016/S0009-2614\(02\)01990-5](https://doi.org/10.1016/S0009-2614(02)01990-5)
- [30] F. Plasser, S. Mai, M. Fumanal, E. Gindensperger, C. Daniel, L. González, *J. Chem. Theory Comput.* **2019**, *15*, 5031–5045. <https://doi.org/10.1021/acs.jctc.9b00525>
- [31] M. Barbatti, *J. Chem. Theory Comput.* **2021**, *17*, 3010–3018. <https://doi.org/10.1021/acs.jctc.1c00012>
- [32] J. R. Mannoouch, J. O. Richardson, *J. Chem. Phys.* **2023**, *158*, 104111. <https://doi.org/10.1063/5.0139734>
- [33] M. Barbatti, K. Sen, *Int. J. Quantum Chem.* **2016**, *116*, 762–771. <https://doi.org/10.1002/qua.25049>
- [34] L. Landau, *Phys. Z. Sowjetunion* **1932**, *2*, 46.
- [35] C. Zener, *Proc. R. Soc. Lond. A* **1932**, *137*, 696–702. <https://doi.org/10.1098/rspa.1932.0165>
- [36] E. Stückelberg, *Helv. Phys. Acta*, **1932**, *5*, 369.
- [37] E. Majorana, *Nuovo Cimento* **1932**, *9*, 43–50. <https://doi.org/10.1007/BF02960953>
- [38] J. C. Tully, R. K. Preston, *J. Chem. Phys.* **1971**, *55*, 562–572. <https://doi.org/10.1063/1.1675788>
- [39] A. K. Belyaev, C. Lasser, G. Trigila, *J. Chem. Phys.* **2014**, *140*, 224108. <https://doi.org/10.1063/1.4882073>
- [40] W. Xie, W. Domcke, *J. Chem. Phys.* **2017**, *147*, 184114. <https://doi.org/10.1063/1.5006788>
- [41] W. Xie, M. Sapunar, N. Došlić, M. Sala, W. Domcke, *J. Chem. Phys.* **2019**, *150*, 154119. <https://doi.org/10.1063/1.5084961>
- [42] J. Suchan, J. Janoš, P. Slavíček, *J. Chem. Theory Comput.* **2020**, *16*, 5809–5820. <https://doi.org/10.1021/acs.jctc.0c00512>
- [43] F. Franco de Carvalho, I. Tavernelli, *J. Chem. Phys.* **2015**, *143*, 224105. <https://doi.org/10.1063/1.4936864>
- [44] M. Mališ, S. Luber, *J. Chem. Theory Comput.* **2020**, *16*, 4071–4086. <https://doi.org/10.1021/acs.jctc.0c00372>
- [45] M. Persico, G. Granucci, *Theor. Chem. Acc.* **2014**, *133*, 1–28. <https://doi.org/10.1007/s00214-014-1526-1>
- [46] S. Mai, P. Marquetand, L. González, *Wiley Interdiscip. Rev. Comput. Mol. Sci.* **2018**, *8*, e1370. <https://doi.org/10.1002/wcms.1370>

- [47] J. Janoš, P. Slaviček, *J. Chem. Theory Comput.* **2023**, *19*, 8273–8284.
<https://doi.org/10.1021/acs.jctc.3c00908>
- [48] L. M. Ibele, B. F. Curchod, *Phys. Chem. Chem. Phys.* **2020**, *22*, 15183–15196.
<https://doi.org/10.1039/D0CP01353F>
- [49] M. A. Kochman, A. Tajti, C. A. Morrison, R. J. D. Miller, *J. Chem. Theory Comput.* **2015**, *11*, 1118–1128. <https://doi.org/10.1021/ct5010609>
- [50] G. R. Medders, E. C. Alguire, A. Jain, J. E. Subotnik, *J. Phys. Chem. A* **2017**, *121*, 1425–1434.
<https://doi.org/10.1021/acs.jpca.6b12120>
- [51] B. F. E. Curchod, A. Sisto, T. J. Martínez, *J. Phys. Chem. A* **2017**, *121*, 265–276.
<https://doi.org/10.1021/acs.jpca.6b09962>
- [52] M. Born, K. Huang, *Dynamical theory of crystal lattices*, New York, Oxford University Press, **1954**.
- [53] A. Abedi, N. T. Maitra, E. K. Gross, *Phys. Rev. Lett.* **2010**, *105*, 123002.
<https://doi.org/10.1103/PhysRevLett.105.123002>
- [54] F. Gatti, B. Lasorne, H.-D. Meyer, A. Nauts, *Applications of Quantum Dynamics in Chemistry*, Springer, Cham, Switzerland, **2017**.
<https://doi.org/10.1007/978-3-319-53923-2>
- [55] J. Coonjobeeharry, K. E. Spinlove, C. Sanz Sanz, M. Sapunar, N. Došlić, G. A. Worth, *Phys. Rev. Lett.* **2022**, *380*, 20200386.
<https://doi.org/10.1098/rsta.2020.0386>
- [56] M. Ben-Nun, T. J. Martínez, *Adv. Chem. Phys.* **2002**, *121*, 439–512. <https://doi.org/10.1002/0471264318.ch7>
- [57] T. J. Martínez, M. Ben-Nun, R. D. Levine, *J. Phys. Chem. A* **1997**, *101*, 6389–6402.
<https://doi.org/10.1021/jp970842t>
- [58] M. Ben-Nun, T. J. Martínez, *J. Chem. Phys.* **1998**, *108*, 7244–7257. <https://doi.org/10.1063/1.476142>
- [59] L. D. Landau, *Phys. Z. Sowjetunion* **1932**, *1*, 51–88.
- [60] J. N. Murrell, S. D. Bosanac, *Introduction to the Theory of Atomic and Molecular Collisions*, Wiley & Sons, Chichester, **1989**.
- [61] C. Wittig, *J. Phys. Chem. B* **2005**, *109*, 8428–8430.
<https://doi.org/10.1021/jp040627u>
- [62] K. Takatsuka, T. Yonehara, K. Hanasaki, Y. Arasaki, *Chemical Theory beyond the Born-Oppenheimer Paradigm*, World Scientific, **2015**.
<https://doi.org/10.1142/9291>
- [63] L. T. A. Ho, L. F. Chibotaru, *Phys. Chem. Chem. Phys.* **2014**, *16*, 6942–6945.
<https://doi.org/10.1039/c4cp00262h>
- [64] A. K. Belyaev, O. V. Lebedev, *Phys. Rev. A* **2011**, *84*, 014701.
<https://doi.org/10.1103/PhysRevA.84.014701>
- [65] M. Sapunar, *Doctoral Thesis*, University of Zagreb, Zagreb, **2021**.
- [66] M. J. Frisch, G. W. Trucks, H. B. Schlegel, G. E. Scuseria, M. A. Robb, J. R. Cheeseman, G. Scalmani, V. Barone, G. A. Petersson, H. Nakatsuji, X. Li, M. Caricato, A. V. Marenich, J. Bloino, B. G. Janesko, R. Gomperts, B. Mennucci, H. P. Hratchian, J. V. Ortiz, A. F. Izmaylov, J. L. Sonnenberg, D. Williams-Young, F. Ding, F. Lipparini, F. Egidi, J. Goings, B. Peng, A. Petrone, T. Henderson, D. Ranasinghe, V. G. Zakrzewski, J. Gao, N. Rega, G. Zheng, W. Liang, M. Hada, M. Ehara, K. Toyota, R. Fukuda, J. Hasegawa, M. Ishida, T. Nakajima, Y. Honda, O. Kitao, H. Nakai, T. Vreven, K. Throssell, J. A. Montgomery, Jr., J. E. Peralta, F. Ogliaro, M. J. Bearpark, J. J. Heyd, E. N. Brothers, K. N. Kudin, V. N. Staroverov, T. A. Keith, R. Kobayashi, J. Normand, K. Raghavachari, A. P. Rendell, J. C. Burant, S. S. Iyengar, J. Tomasi, M. Cossi, J. M. Millam, M. Klene, C. Adamo, R. Cammi, J. W. Ochterski, R. L. Martin, K. Morokuma, O. Farkas, J. B. Foresman, D. J. Fox, *Gaussian 16*, **2016**.
- [67] E. Runge, E. K. U. Gross, *Phys. Rev. Lett.* **1984**, *52*, 997–1000.
<https://doi.org/10.1103/PhysRevLett.52.997>
- [68] M. Casida, *Recent Advances in Density Functional Methods, Part I*, World Scientific, Singapore, **1995**.
- [69] M. Petersilka, U. J. Gossmann, E. K. U. Gross, *Phys. Rev. Lett.* **1996**, *76*, 1212–1215.
<https://doi.org/10.1103/PhysRevLett.76.1212>
- [70] J. P. Perdew, K. Burke, M. Ernzerhof, *Phys. Rev. Lett.* **1996**, *76*, 3865–3868.
<https://doi.org/10.1103/PhysRevLett.77.3865>
- [71] H. Iikura, T. Tsuneda, T. Yanai, K. Hirao, *J. Chem. Phys.* **2001**, *115*, 3540–3544.
<https://doi.org/10.1063/1.1383587>
- [72] X.-R. Ma, J. Zhang, Y.-C. Xiong, W. Zhou, *Mol. Phys.* **2022**, *120*, e2051761.
<https://doi.org/10.1080/00268976.2022.2051761>